Applied Catalysis B: Environmental 203 (2017) 615–624

Contents lists available at ScienceDirect

Applied Catalysis B: Environmental

journal homepage: www.elsevier.com/locate/apcatb

Effective surface disorder engineering of metal oxide nanocrystals for improved photocatalysis

Liangxu Lin[a], Juntong Huang[a,b], Xifei Li[c], Monsuru A. Abass[d], Shaowei Zhang[a,*]

[a] College of Engineering, Mathematics and Physical Sciences, University of Exeter, Exeter EX4 4QL, UK
[b] School of Materials Science and Engineering, Nanchang Hangkong University, Nanchang 330063, China
[c] College of Physics and Materials Science, Tianjin Normal University, Tianjin 300387, China
[d] Mechanical and Nuclear Engineering Department, Kansas State University, Manhattan, KS, 66506, USA

ARTICLE INFO

Article history:
Received 6 July 2016
Received in revised form 14 October 2016
Accepted 18 October 2016
Available online 19 October 2016

Keywords:
Surface disorder
Photocatalyst
Titanium dioxide
Zinc oxide
Indium oxide

ABSTRACT

Metal oxide (MO) semiconductors such as titanium dioxide (TiO_2) are often used in many photochemical processes (*e.g.* waste-water remediation). However, their large band gaps limit their catalytic performances. Various techniques have been developed to improve the photocatalytic activity of TiO_2 nanocrystals (NCs), *e.g.*, *via* chemical doping, designing hybrid electronic structures, and creating surface disorders. Unfortunately, these techniques suffered from various disadvantages including complex/expensive operations and still poor photoactivity of modified TiO_2 under near-infrared (IR) light (53% of the full solar irradiation). Here, we demonstrate a simple but universal route to introducing continous internal energy levels in MO semiconductors, including TiO_2, zinc oxide (ZnO) and indium oxide (In_2O_3) NCs. This new technique just requires simply heating a mixture of an MO NC with potassium (K). Distingctly from conventional MO NCs, NCs prepared using the present technique were all in black color and able to adsorb nearly full solar spectrum. As-prepared black TiO_2 NCs performed >300 times better than their conventional counterparts in the photocatalytic degradation of methylene blue (MB) dye under visible light irradiation. Similar levels of improvements in the photocatalytic performance were also achieved with as-prepared ZnO and In_2O_3 NCs. In addition, we show how NCs could be changed to black ones with tailored electronic structures. Our results suggested that the improvements in the NC's photoactivity were mainly attributed to the surface disorder induced, oxygen (O) vacancies and metallic phases likely formed during the reaction process with K.

1. Introduction

As cost-effective semiconductors, metal oxides (MOs) such as TiO_2 and ZnO have been extensively investigated for various photocatalytic processes such as waste-water remediation, self-cleaning surfaces, and clean energy production (*e.g.* water splitting), because of their ability to capture and transfer abundant natural solar energy to chemical energy [1–12]. Unfortunately, due to their intrinsic large band-gaps, their light absorption efficiency is poor [13]. For example, TiO_2 has a band gap of ~3.2 eV and can only absorb UV light (only <4% of the full solar spectrum) [14]. The efficiency in utilization of the solar energy is further lowered when a nanosized MO is used (due to quantum confinement effect) though its high surface areas could be beneficial to a surfacial catalytic process.

The light absorption of MOs, in the case of catalysis, could be improved by designing a composite with a hybrid band structure [15,16] or introducing defects *via* chemical doping [17,18]. Although these two techniques could narrow down the band gap of MO *via* formation of new internal energy levels, the introduced defect levels are discontinuous and thus only active to specific narrow light regions. For this reason, the modified MO materials were usually not effective enough in utilizing solar light for photocatalytic reactions. Recently, a more promising approach was suggested for introducing continuous defect levels in TiO_2 to improve its photoactivity, *via* surface disorder and modification achieved by hydrogenation [12,19], Al/CaH_2 reduction [20,21], and other similarly-derived routes [22–25]. Nevertheless, the implementation of these techniques is still being hindered by several factors including a prolonged reaction time (5 days) [12], high processing temperature (*e.g.* 500 °C) [20,21], and poor light utiliza-

* Corresponding author.
E-mail address: s.zhang@exeter.ac.uk (S. Zhang).

http://dx.doi.org/10.1016/j.apcatb.2016.10.054
0926-3373/

tion efficiency in the near-infrared (IR) region (which accounts for nearly 53% of the full solar spectrum) [17]. Although some other improved routes (*e.g.* hydrogen plasma assisted chemical vapor deposition [26], water plasma assisted synthesis [27], magnesiothermic reduction with H_2 at a temperature as high as 650 °C [28]) were also attempted to disorder the surface of TiO_2, they were very complex and expensive. Moreover, few of these techniques have been demonstrated to be universally applicable to the cases of other MOs (*e.g.* ZnO and In_2O_3).

In this paper, we report a simple but more effective and universal technique based on surface disorder engineering, by which conventional MO nanocrystals (NCs) can be converted into excellent full solar light absorbers for photocatalytic reactions. The key step of this new technique is just simply mixing and heating an MO (TiO_2, ZnO and In_2O_3) NC with K. Although the reaction process is simple, it is very effective in forming MO NCs having various surface disorders, O vacancies, and considerably improved light absorbance in the full visible-near IR region. Differently from conventional MO NCs, all the as-prepared NCs were in black color and showed considerably improved photocatalytic performances.

2. Experimental

2.1. Materials

The main raw materials used included TiO_2 NCs (<25 nm, product No. 637254), In_2O_3 NCs (<100 nm, product No. 632317), MB (product no: M9140), methylene orange (product no: 114510), K (product no. 244864), $NaNO_2$ (product no: S2252) and KCl (product no. p9333), from Sigma-Alrdich, and ZnO NCs (10–30 nm, product No. US3590) from US Research Nanomaterials, Inc. Absolute ethanol (EtOH) and acetone were purchased from Fisher Scientific, and distilled water was prepared in our own laboratory.

2.2. Preparation of black MO NCs

For the preparation of black TiO_2, initially ~0.6 g K was put into a Pyrex tube with side connections to a vacuum pump. 1 g of white anatase TiO_2 NC was placed quickly into the tube and then vacuumed (10^{-3} Torr). Intense reaction between the NC and K was observed upon gently shaking the tube, and most of the original white NC was changed rapidly to black in just a few seconds. The tube was then kept at 140 °C in a silicon oil bath (heated by a hot plate) for 1 h to allow the reaction to be completed (*i.e.,* until no original white powder remained). After the tube was cooled to room temperature, 20 mL absolute EtOH was poured into the Pyrex tube to safely react with K phases. The resultant black product was washed with 30 mL EtOH before being transferred to a 200 mL beaker. The black powder was collected *via* centrifugation, and washed repeatedly with 1:1 (volume ratio) EtOH/H_2O solvent until pH value of the dispersed product was close to 6 (the pH value of distilled water used), and finally dried for later use.

Preparation and purification procedures for black In_2O_3 were the same as those used for black TiO_2, except 3 g of faint yellow In_2O_3 were reacted with 0.9 g K. As for the black ZnO, 1 g white ZnO was reacted with 0.6 g K at ~170 °C for 2 h. Its purification procedure was slightly different from that for black TiO_2 or In_2O_3 NCs. Upon black ZnO being transferred to a 200 mL beaker, 1:4.5:4.5 acetone/EtOH/H_2O (volume ratio) was used to wash away the residual K. The resultant black ZnO was rinsed with pure acetone, air-dried and then stored for later use.

2.3. Characterization

X-ray diffraction (XRD) analysis was carried out using a Bruker D8 Advance diffractometer with Cu Kα radiation (λ ~ 0.154 nm, 40 kV, 40 mA) at 2° (2θ)/min. For comparison, identical amounts of as-received NCs and as-prepared black NCs were used for XRD. Raman spectra of samples were recorded using a Renishaw Raman spectrometer with an excitation wavelength of 532 nm (2 mW laser). Since Raman response from as-received NCs was much stronger than that from as-prepared black NCs, for better comparison, 1% and 10% laser powers were used respectively for the cases of the former and the latter. 10% laser power was also used in the measurement of as-received NCs to confirm that the fine Raman response was the same as that in the case of using 1% laser power. The Raman peak of pure Si wafer at 520 cm^{-1} was used to calibrate all the Raman modes of the NCs. Micro- and crystalline-structures of the NC samples were examined using a JEOL JEM-2100 TEM at an accelerating voltage of 200 kV. A Shimadzu-3600 spectrometer was used to record the UV/Vis absorption spectra (Fig. S6a) of as-received NCs (dispersed in distilled H_2O, in quartz cuvette with 1 cm light path). However, for UV/Vis-near IR diffusive reflectance and transmittance spectra (Figs. 3a, 6a and b, Fig. S3 and Fig. S6b–d) of NCs, a Shimadzu ISR-603 Integrating sphere attachment was used. In this measurement (200–2500 nm), identical amounts of as-received and as-prepared NCs were pressed respectively in the sample holder (with a standard scan speed). To investigate the absorption tail in the near IR region (Fig. S6b–d), a very slow scan rate was used to alleviate the influence from the instrument response and environmental background. The Shimadzu-3600 spectrometer was also used to measure the characteristic absorbance of the MB and methylene orange dye in the photocatalysis studies (no integrating sphere was used; the dye solution was measured in quartz cuvette with 1 cm light path). XPS was performed on a Kratos AXIS Nova X-ray photoelectron spectrometer with an excitation source of Al Kα. The binding energy of XPS was calibrated based on C1s (284.6 eV). AC impendence measurements of NCs were carried out using a CHI 650C electrochemical workstation with three electrodes [reference electrode: Ag/AgCl, 1 M KCl, E (potential) = 0.235 V *versus* RHE; counter electrode: Pt; working electrode: glassy carbon (0.003 m effective diameter)], at an overpotential of 100 mV and a frequency between 10^5 Hz and 0.01 Hz with an AC voltage peak of 1 mV. Photo-generated current was measured using a 0.5 M KCl electrolyte. Identical amounts (~10 mg) of as-received and as-prepared black NCs were deposited respectively on 1 × 1 cm^2 ITO and air-dried. The measurement was performed with a bias voltage of 0.1 V with and without AM 1.5G solar light illumination (Newport Oriel full spectrum solar simulator, 92250A-1000, 1.5 G, 150 W Xenon lamp) in an otherwise dark environment. The measurement of incident photon conversion efficiency (IPCE) was performed in air with an Oriel QE/IPCE measurement kit. N_2 gas adsorption/desorption isotherms were determined using a Quantachrome Autosorb-iQ gas sorptometer *via* the conventional volumetric technique. The Brunauere-Emmette-Teller (BET) surface area was calculated based on adsorption data in the partial pressure (P/Po) range of 0.02–0.22.

2.4. Evaluation of photocatalytic performance

Solar-driven photocatalysis measurements were conducted by irradiating samples with a Newport Oriel full spectrum solar simulator (92250A-1000, 1.5 G, 150 W Xenon lamp). The average intensity of solar irradiation onto the solution was measured as 5.2 mW cm^{-2} by the ILT 550-RAA spectroradiometer at 9 different spots. 50 mg black NCs and 100 mL 20 ppm MB or methylene orange (50 mL 40 ppm MB or methylene orange was diluted with 50 mL NCs suspension) were placed in a beaker (inner diameter: 5 cm) to evaluate the catalytic performance. Control measurements of MB or methylene orange were carried out under the identical conditions but 50 mg white NCs or no NCs were used. To achieve only visible light irradiation, a 1 M aqueous solution of $NaNO_2$ was used

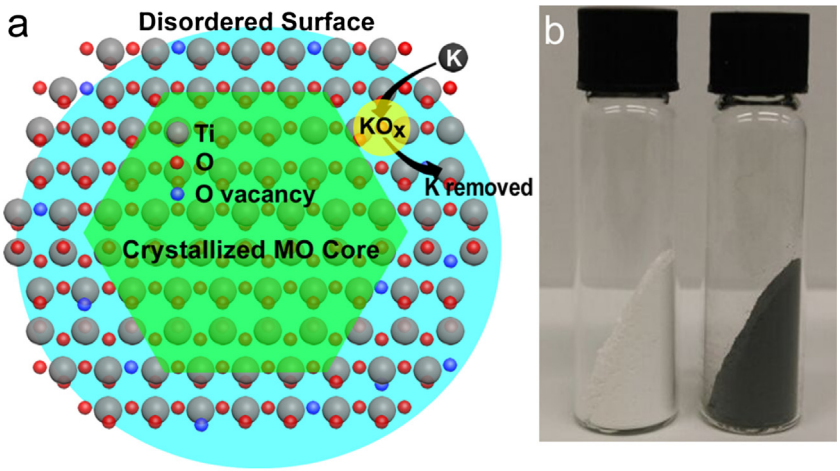

Fig. 1. (a) Scheme of the reaction between TiO_2 NC and K. K diffused inwardly and reacted with O in the crystal lattice, resulting in crystal disorders on the NC's surface. K in the disordered lattice of NC was further reacted and washed away, and the disordered surface of NC remained. (b) Photographs of TiO_2 NCs before (left image) and after (right image) surface disorder engineering.

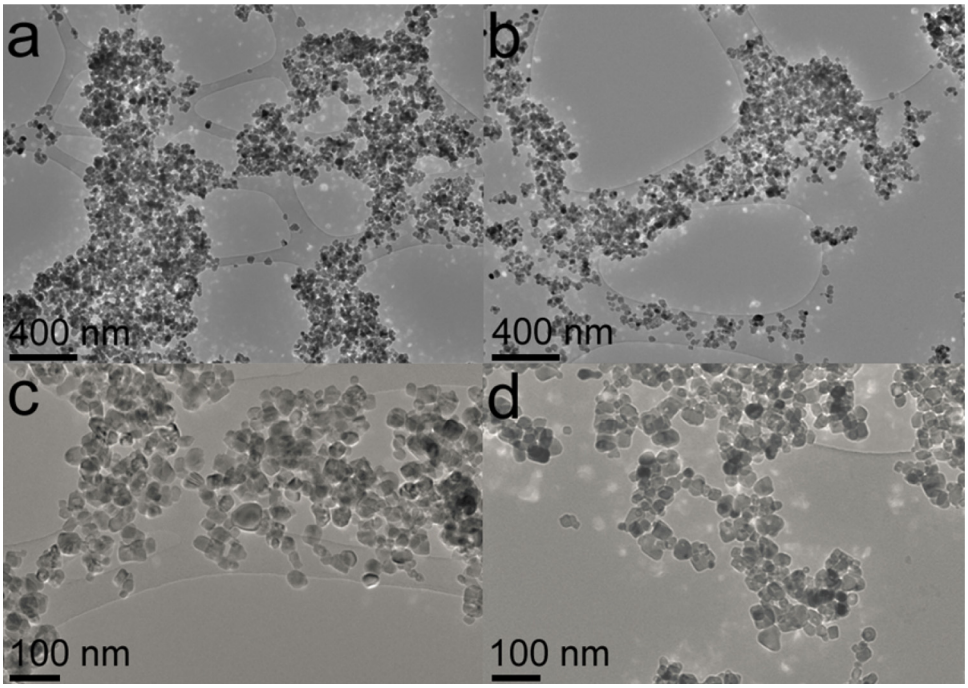

Fig. 2. TEM images of (a,c) as-received white- and (b,d) as-prepared black-TiO_2 NCs.

to filter out all the UV lights under 390 nm (Fig. S1). To examine the adsorption of MB by NCs, dark experiments (without any light irradiation) were also carried out similarly. A syringer (attached with a filter paper) was used to remove the majority of NCs and transfer the solution for UV/Vis measurement.

3. Results and discussion

To illustrate the fundamental principle of the new technique and its universality, we initially describe how to convert white TiO_2 NCs to their black counterparts and how such a conversion affects their photocatalytic performance, and then demonstrate how such a principle can be further extended to other cases of MO-NCs (*e.g.* ZnO and In_2O_3). During the modification of TiO_2 NCs, an intense reaction between TiO_2 NCs and K was observed (the NCs were also changed to black) upon gently shaking the tube at room temperature. It is believed that this reaction occurred mainly between highly active surface oxygen (O) of the small TiO_2 NCs (<25 nm) and K (Fig. 1a, K can react with O of TiO_2 to form KO_x). To confirm this, we also used "coarser" TiO_2 NCs (<100 nm) to replace the small TiO_2 NCs, but no white-to-black conversion was observed, unless the mixture was heated up to above 70 °C. Similarly to the K intercalation in layered materials [29–32], K was also intercalated into the lattice of TiO_2, and diffused inwardly at a relatively high temperature (*e.g.* 140 °C used here). After the completion of the intercalation reaction, the intercalated K at the disordered sites (this will be further confirmed in Fig. 4) and the residual/unreacted K were washed away by initially pure EtOH and then EtOH/H_2O (1:1) (similar to that used previously for the K-deintercalation in layered materials [29–32]), resulting in desired black TiO_2 NCs (Fig. 1b).

The resultant black TiO_2 NCs did not show much size change, compared to the as-received NCs (Fig. 2a and b). Closer exam-

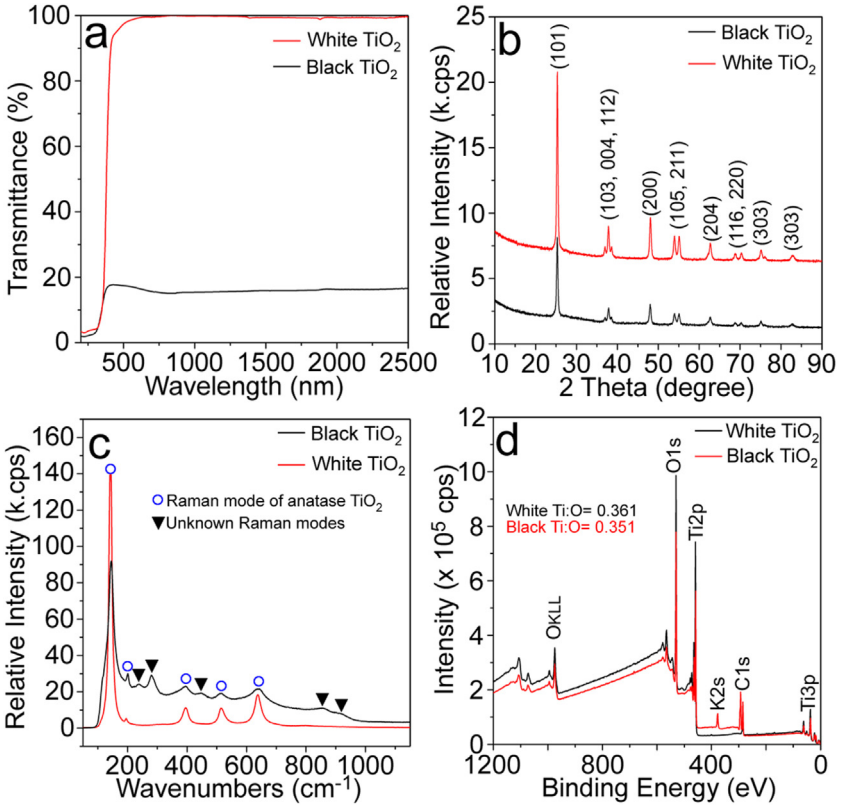

Fig. 3. Characterization of as-received white and as-prepared black TiO_2 NCs (the same amounts of white and black NCs were used in each case). (a) UV/Vis-near IR diffusive reflectance and transmittance spectra; (b) XRD patterns; (c) Raman spectra; (d) XPS full survey.

inations revealed that they were only slightly smaller (with an average size around 19.8 nm, Fig. 2d and Fig. S2b) than the original white NCs (with an average size around 20.4 nm, Fig. 2c and Fig. S2a). This was reasonable as some severely reacted and disordered surface of TiO_2 most likely had been exfoliated with the K removal (KOx reacted with $EtOH/H_2O$ and generated H_2, Fig. 1a). As-prepared black TiO_2 NCs were quite stable. They did not show any color change even after having been exposed to the atmosphere for >1 year.

The white-to-black color change of TiO_2 NCs after the simple process described above was reflected by their diffusive reflectance and transmittance spectra (collected through an integrating sphere, see "**Characterization**"). As shown in Fig. 3a, both as-received white- and as-prepared black TiO_2 NCs showed strong absorptions at ~300 nm (the corresponding absorption spectra are shown in Fig. S3a). However, compared with the former, the latter showed considerably improved absorption at longer wavelengths (from 400 to 2500 nm, Fig. 3a and Fig. S3a). The visible light (from 390 to 780 nm, 43% of the solar spectrum) absorption of the black TiO_2 NCs was close to 90% (Fig. 3a), whilst the white NCs were nearly transparent in this region (showing only a weak absorption tail from 400 to 550 nm). Differently from black TiO_2 prepared previously *via* hydrogenation, which only showed improved visible light absorbance to ~810 nm [12], black TiO_2 NCs prepared in this work were also photoactive in the near-IR light region (from 780 to ~2500 nm), with around 88% absorption (Fig. 3a). This demonstrated that black TiO_2 NCs prepared in this work were photoactive nearly for the full solar spectrum, which was similar to that observed in the case of colored TiO_2 created *via* Al/CaH_2 reduction at a high temperature (*e.g.* 500 °C) [20,21].

We examined the crystalline structures of TiO_2 NCs using XRD and Raman spectroscopy (the same amounts of white and black NCs were used in each case). As-prepared black TiO_2 NCs exhibited the same anatase crystal structure (JCPDS: 21-1272) as that of as-received white TiO_2 NCs, but their diffraction peaks were much weaker (50% lower than in the case of the latter, Fig. 3b), indicating that the NC crystal structure in the former had been disordered. This was further verified by Raman examinations. According to Fig. 3c, both types of NCs showed characteristic Raman modes of anatase TiO_2 at around 145, 197, 395, 515, 518 (superimposed with the 514 cm^{-1} band), and 638 cm^{-1} [12]. All these modes were broader in the case of black NCs than in the case of white NCs, due to the crystal disorder. In addition, black TiO_2 NCs showed five unknown Raman modes at around 238, 280, 447, 854 and 916 cm^{-1}, indicating that their structure disorder resulted in new zone-edge and other Raman-forbidden modes by breaking down the Raman selection rule. Nevertheless, XPS full survey (Fig. 3d) revealed that chemical composition of black TiO_2 NCs remained close to the original one, with only slight difference in O content. In the spectrum, a weak peak from K appeared, due to minor K impurities remained in the sample. Due to the surface-adsorbed O, the ratio of Ti:O became lower than 0.5, but this was very useful for the later determination of O vacancies in the NCs (see Fig. 10). More specific changes in the crystal structure can be revealed by high-resolution TEM (HR-TEM). As shown in Fig. 4a and b, as-received TiO_2 NCs were highly crystallized, showing clear lattices. By contrast, black NCs showed highly disordered surface and crystalline core (Fig. 4c and d), explaining well their reduced crystalline extent.

To understand how such surface disorder affected the NC's performance in photo-chemical processes (*e.g.* photocatalysis), we evaluated the catalytic activity of as-prepared black TiO_2 NCs in the photocatalytic degradation of an MB solution, *via* monitoring the change of light absorbance at the 665 nm wavelength (the main characteristic absorption peak of MB). 50 mg of NCs were dispersed (in 50 mL deionized water contained in a beaker with an inner diameter of 5 cm) under magnetic stirring at room temperature

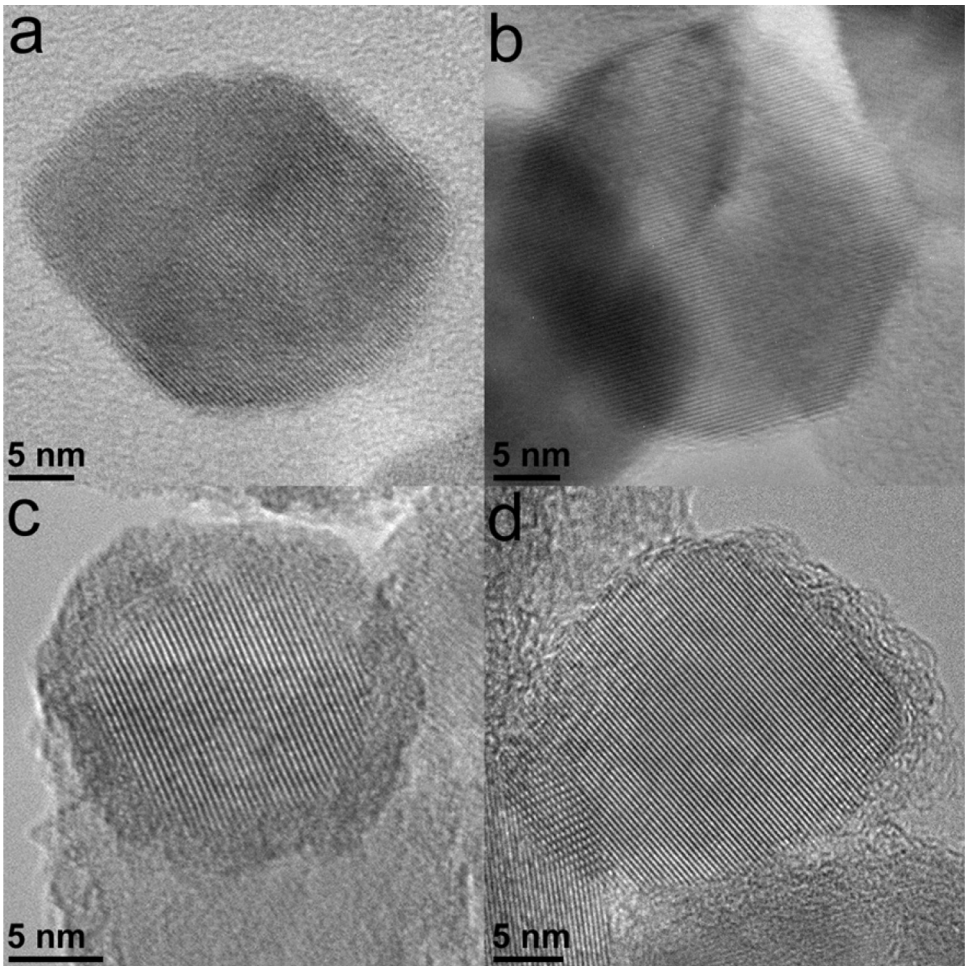

Fig. 4. HRTEM images of (a,b) as-received white and (c,d) as-prepared black TiO_2 NCs.

(20 °C), and exposed to simulated solar irradiation (5.2 mW cm^{-2}). Then, 50 mL of 40 ppm fresh MB were added to the beaker to achieve an overall concentration of 20 ppm and an initial optical density (OD_{665}) of 1.87 (the background of NCs was subtracted). Control measurements on MB under the identical conditions were also performed with 50 mg white TiO_2 NCs or without using any NCs. When no NCs were used, the photodegradation of MB under solar light irradiation was slow (*e.g.* only 50% was degraded after 440 min, Fig. 5a, Fig. S4a). When white TiO_2 NCs were used, all the MB degraded completely after 160 min (the self-photodegration of MB was 15%, also see Fig. S4a). Finally, when black TiO_2 NCs were used, all the MB degraded completely after only 14 min [Fig. 5a; the self-photodegration of MB in the 14 min was negligible (only ~1.0%), Fig. S4a]. In the case of using black TiO_2 NCs, >87% and 98% MB were photodegradated in 1 and 2 min, respectively (the self-photodegration of MB in 1 and 2 min was 0.08 and 0.17%, respectively, see Fig. S4a).

We also carried out a control experiment to understand the adsorption of MB on the surface of black NCs in dark environment. The results showed that the adsorption of MB on black TiO_2 NCs was little (<3.0%) after 2 min stirring, although it increased slightly to ~4.4% after 20 min (Fig. S4c). Based on these adsorption results and self-photodegradation of MB, the actual photo-degradation of MB catalyzed by black TiO_2 NCs in 2 min, was calibrated as >94.8%. This, along with the short time (14 min) required for complete photodegradation of the MB (MB: 100 mL, 20 ppm; catalyst: 50 mg; solar light intensity: 5.2×10^{-3} W cm^{-2}), indicated that TiO_2 NCs prepared in this work were 2.5 times more effective than hydrogenated black TiO_2 NCs (MB: 3 mL, 10.7 ppm; catalyst: 0.15 mg; solar light intensity: 0.1 W cm^{-2}; complete degradation time: 8 min) [12]. The improvement in the solar-driven catalytic performance (>10 times) from pristine white TiO_2 NCs was also greater in the present case than in the cases of using other previously reported modification methods (about 5 times improvement in the cases of hydrogenated black TiO_2 NCs [12] and Al reduced colored TiO_2 NCs, from pristine white TiO_2 NCs [20]).

The improved catalytic performance of black TiO_2 NCs from the original white TiO_2 became more evident when a visible-infrared light irradiation was applied. We used 1 M $NaNO_2$ aqueous solution to filter out all the lights with a wavelength <390 nm (Fig. S1). In this case, the MB remained stable and no obvious self-photodegradation was observed (Fig. 5b and Fig. S4b). The MB was completely photo-degraded after about 5300 min if stoichiometric white TiO_2 NCs were used. However, upon using black TiO_2 NCs, photo-degradation of MB was completed in just 17 min (such a catalytic efficiency was >300 times greater than that in the case of using white NCs). The time (17 min) required in this case was close to that (14 min) in the case of under solar light irradiation, indicating the much greater photoactivity of black NCs in the visible-near infrared light region (the main component, >96%, of the natural solar light). We further performed cyclic tests on the solar-driven degradation of MB catalyzed by as-prepared black TiO_2 NCs. After the complete degradation of MB in the previous cycle, black TiO_2 NCs were collected, washed with ethanol, dried in oven (at 80 °C) and then re-used for the next cycle of test. The good repeatability in the photodegradation of seven cycles (Fig. 5c) demonstrated

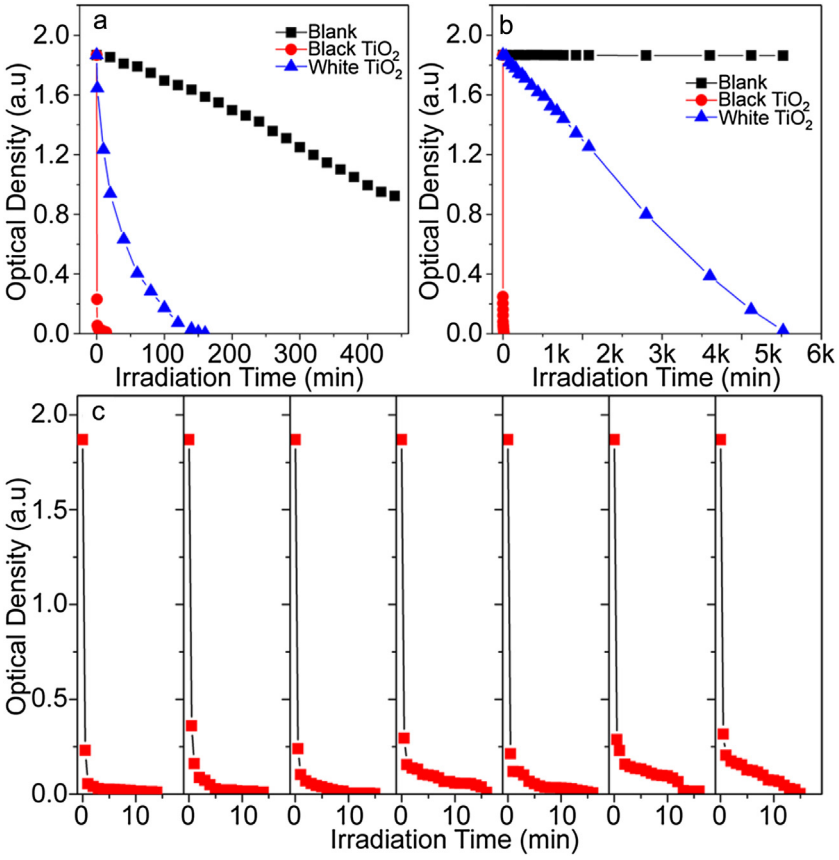

Fig. 5. Photocatalytic performance. (a) Degradation of MB (20 ppm, 100 mL) under solar light irradiation with black, white TiO_2 NCs and without any NCs. (b) Degradation of MB (20 ppm, 100 mL) under visible light irradiation (UV light was filtered out by using 1 M $NaNO_2$ aqueous solution) with black, white TiO_2 NCs and without any NCs. (c) Cyclic tests of solar-driven photocatalytic activity (MB degradation) of as-prepared black TiO_2 NCs. Data in the figure were from the first 20 min measurements in each of the seven consecutive photodegradation testing cycles.

that the photocatalytic activity of black TiO_2 NCs remained stable under solar irradiation. Ever after being left in the atmosphere for >1 year, as-prepared black TiO_2 NCs still retained their excellent catalytic activity (as shown in Fig. S4d, the MB was completely photodegraded after 14 min). They showed only slight degeneration at the start of the catalysis process (Fig. S4d, >92% MB was photodegraded in 2 min. This was only slightly less than that (98% MB) in the case of using freshly prepared black NCs). In addition, as-prepared black TiO_2 (50 mg) showed high catalytic activity in the degradation of methylene orange (20 ppm, 100 mL, complete degradation in 18 min), which was much better than that of as-received white NCs (Fig. S5a, only <6.8% methylene orange was degraded in 18 min).

The improved photocatalytic performance of black TiO_2 NCs was attributable to the surface disorder (color change of TiO_2 NCs) induced during their preparation processes. Based on the similar principle, various other types of MOs with large bandgaps (so mainly absorb UV light) also can be similarly activated for absorbing a visible-near IR light, improving considerably their solar-driven photocatalytic efficiencies. To further illustrate this, ZnO and In_2O_3 black NCs were similarly prepared using white ZnO (10–30 nm) and faint yellow In_2O_3 NCs (<100 nm) as starting raw materials (see "**Experimental**" section). As in the preparation of black TiO_2 NCs, these as-received NCs also could be readily changed to the corresponding black NCs with improved absorbance in the visible-near IR region (Fig. 6a & b, also see the absorbance spectra in Fig. S3b and c).

As in the case of TiO_2 NCs, XRD (Fig. 6c and d) confirmed that ZnO and In_2O_3 NCs with disordered structure had been prepared. As seen from Fig. 6c, all the diffraction peaks from as-received (original) and as-prepared ZnO NCs (the same amounts of NCs were used for the XRD analysis) can be assigned to hexagonal ZnO (JCPDS: 89-7102), but the diffraction peaks from black ZnO NCs became much weaker than those from as-received ZnO. XRD also confirmed the cubic structure (ICDD: 65-3170) of as-received and as-prepared In_2O_3 NCs (Fig. 6d; the same amounts of NCs were used for the measurements), and the weaker diffraction peaks of black In_2O_3 NCs than those from as-received In_2O_3 NCs. Fig. 7 presents Raman spectra of ZnO and In_2O_3 NCs. Apart from the same/similar Raman modes from as-received and as-prepared NCs, several unknown Raman modes were also observed in the case of black NCs, which arose from the structure disorder (corresponding well to the XRD results). The surface disorder was further confirmed by HRTEM observations. As shown in Fig. 8, as-received ZnO and In_2O_3 NCs were highly crystallized. As for their black counterparts, they exhibited a "core-shell" structure. The crystalline extent of the core part was degenerated, and the shell part clearly became disordered, *i.e.*, amorphous.

Such structural changes of NCs could be already greatly beneficial to their photocatalytic activities. To confirm this, we investigated the catalytic degradation of MB using ZnO and In_2O_3 NCs following the same protocol as that in the case of TiO_2 NCs. As shown in Fig. 7c and d, photocatalytic degradation of MB (20 ppm, 100 mL) using as-received white ZnO or faint yellow In_2O_3 NCs (50 mg) was slow, requiring 95 and 110 min respectively to

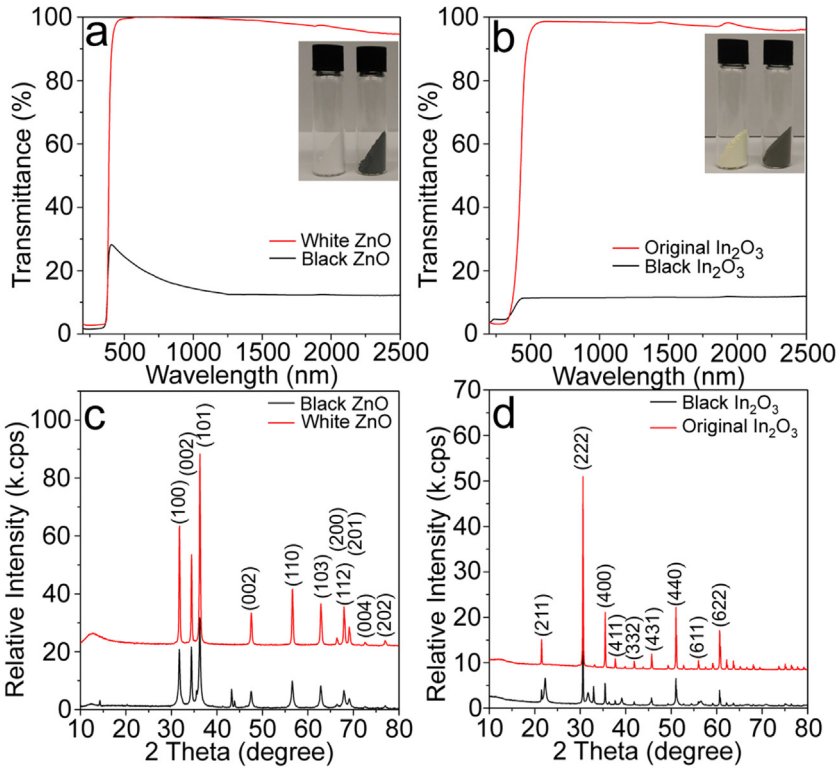

Fig. 6. UV/Vis-near IR diffusive reflectance and transmittance spectra of (a) as-received *versus* as-prepared ZnO, and (b) as-received *versus* as-prepared In_2O_3 NCs. Characterizations were performed on pressed samples containing the same amounts of NCs. Inset images are photographs of as-received (left) and as-prepared black NCs (right). (c) XRD patterns of white (hexagonal, JCPDS: 89-7102) and black ZnO NCs. (d) XRD patterns of as-received (cubic, JCPDS: 65-3170) and as-prepared black In_2O_3 NCs.

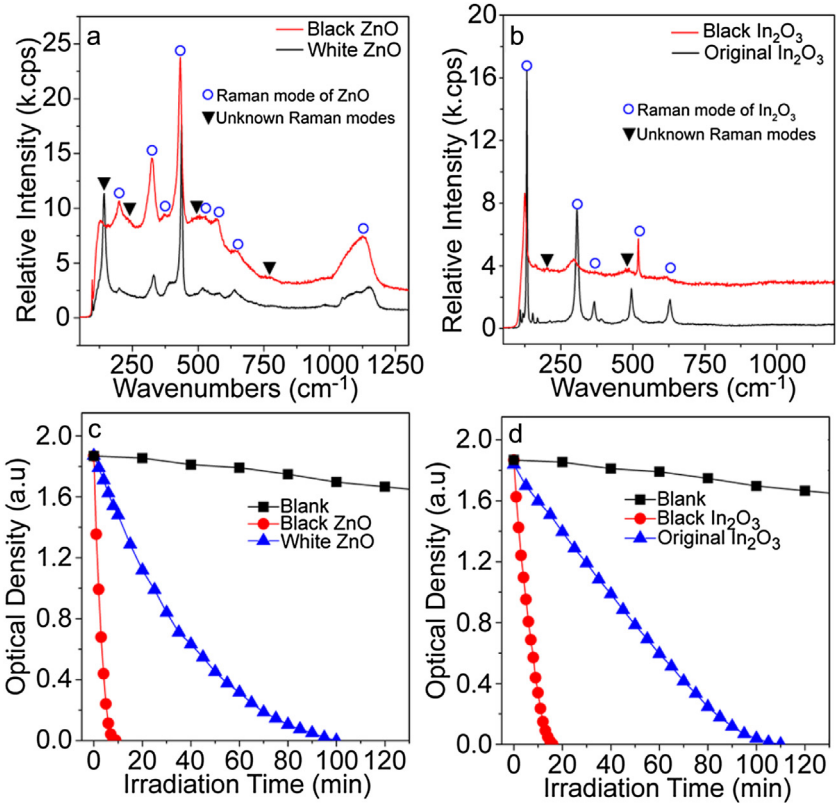

Fig. 7. (a) Raman spectra of as received white and as-prepared black ZnO NCs. (b) Raman spectra of as-received and as-prepared black In_2O_3 NCs. (c) Degradation of MB (20 ppm, 100 mL) under solar light irradiation with black, white ZnO NCs and without any NCs. (d) Degradation of MB (20 ppm, 100 mL) under solar light irradiation with black, faint yellow (original) In_2O_3 NCs and without any NCs.

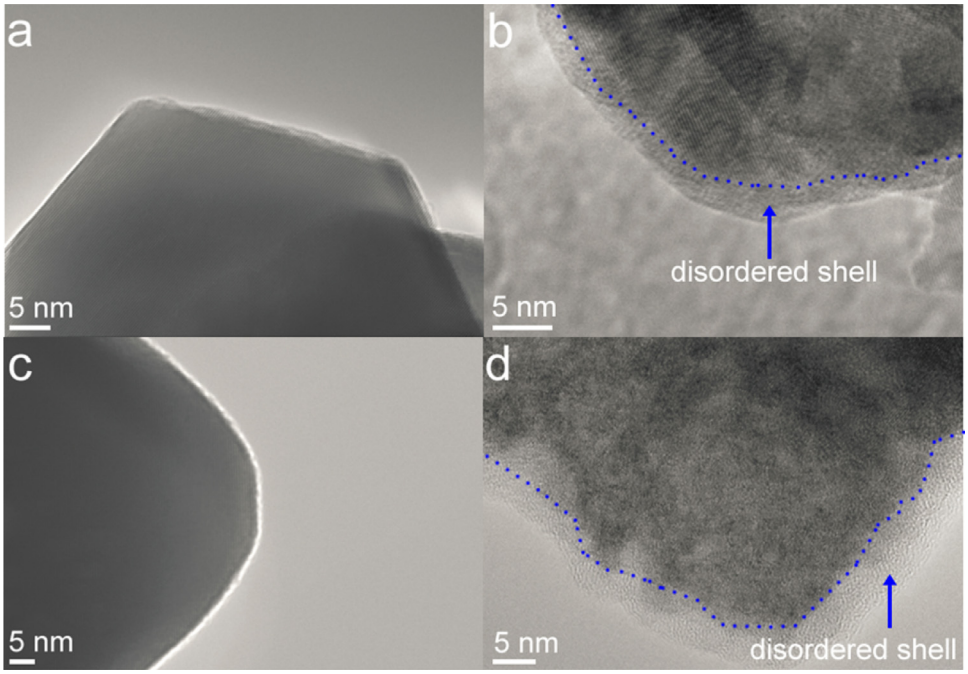

Fig. 8. HRTEM images of, (a) as-received white and (b) as-prepared black ZnO NC, and (c) as-received and (d) as-prepared black In_2O_3 NC. As-received ZnO and In_2O_3 raw materials were highly crystallized. However, after the processing, the part close to their surface became evidently disordered.

complete the degradation under the solar light irradiation. Self-degradation of MB without using NCs was 8.6% after 95 min, and increased to 10.1% after 110 min (Fig. 7c and d, also see Fig. S4e and f). On the other hand, when black ZnO and In_2O_3 were used, degradation of MB was completed after just 8 and 10 min, respectively. The results from our dark control experiments revealed that the adsorption of MB using both types of NCs was low, <3.0 and <4.3% after 2 and 20 min, respectively (Fig. S4c). Self-photodegradation of MB on this time scale was neglectable, only 0.6% after 8 min and 0.75% after 10 min, suggesting that over 95.1% and 94.9% MB (100 mL, 20 ppm) were catalytically degraded after respectively 8 and 10 min, by using 50 mg black ZnO and In_2O_3 NCs. This result indicated excellent photocatalytic performance of black ZnO/In_2O_3 NCs, which was close to that of black TiO_2 NCs (Fig. 5a). More straightforwardly, we used methylene orange (20 ppm, 100 mL) to further evaluate the catalytic activity of black ZnO and In_2O_3 NCs (50 mg, Fig. S5b and c). The time required for complete catalytic degradation of methylene orange was only 22 and 26 min, when black ZnO and black In_2O_3 NCs were used respectively, indicating significant improvements in the catalytic activity in both cases, compared to in the cases of using as-received NCs (<4.5% and <1.3% methylene orange were degraded after 22 and 26 min, respectively, by using as-received white ZnO NCs and In_2O_3 NCs).

To assist understanding the reasons behind the above findings (in particular, why the black NCs exhibited considerably improved photocatalytic activity), we further investigated electronic structures of the NCs. As shown by the Tauc plots [30,33] of dispersed NCs (the corresponding UV/Vis absorption spectra are shown in Fig. S6a), the optical band gaps of as-received TiO_2, ZnO and In_2O_3 NCs were around 3.29, 3.24 and 3.20 eV, respectively. The diffusive reflectance and absorbance spectra of black TiO_2 NCs showed a clear absorption tail at around 2730 nm, whilst white TiO_2 NCs were photo inactive in this light region (Fig. S6b). The Tauc plot from this absorption spectrum of black TiO_2 NCs gave an indirect optical band gap of 0.45 eV (Fig. 9b).

The diffusive reflectance and absorbance spectra of black ZnO and In_2O_3 NCs also showed an absorbance tail at around 2592–2695 nm (Fig. S6c and d). By using the same method as that in the case of black TiO_2 NCs (Tauc plots, Fig. 9b), the indirect optical band gaps of black ZnO and black In_2O_3 NCs were determined as around 0.46 and 0.48 eV, respectively. XPS valence states of these NCs (both as-received NCs and as-prepared black NCs) gave more details about the valence (VB) and conduction band (CB) shifts arising from the engineered surface disorder. Fig. 9c, as an example, shows that the VB of surface disordered (black) TiO_2 up-shifted by about 0.32 eV from that of white TiO_2, implying that the CB tail of the black TiO_2 down-shifted from that of white TiO_2 by about 2.52 eV (also see the illustration in Fig. 9d). Black ZnO and In_2O_3 NCs showed similar changes in the band position, with VB upshift by ~0.36 and ~0.7 eV (Fig. S6e and f), and CB downshift by 2.42 and 2.02 eV, respectively. Previous studies revealed that the surface disorder of TiO_2 induced *via* hydrogenation led to the uplift in its VB [12,19,23,34]. However, the uplifts of VB (by 0.32–0.7 eV) were not significant enough to explain the photo activities of all the three types of black NCs in the near-IR region. Theoretical and experimental studies [12,19,34,35] have confirmed that with the surface disorder of MOs, various levels of defects were also created between CB and VB, and the CB position was downshifted. Nevertheless, compared with previously-prepared TiO_2 with surface disorders [12,19,22,34,35], black NCs prepared in this work had a much narrowed band gap, suggesting that the simple reaction between NC and K was more capable of introducing such continuous defect levels near and under CB.

In as-prepared black NCs, we also found significant oxygen (O) vacancies, which further enhanced the internal defect levels [4,19,36]. This can be illustrated by taking the case of TiO_2 NCs as an example. Fig. 10 gives O1s XPS of white and black TiO_2 NCs. The binding energies of 530.1 and 531.1 eV can be assigned respectively to Ti-O and adsorbed O on the surface [37]. In the case of white TiO_2 NCs, based on their O1s XPS, the ratio of Ti-O (O in TiO_2 NCs)/O (total O including that surface adsorbed) was determined as 72.65%. Considering the ratio of Ti/O (0.361) given by the XPS full survey (Fig. 3d) and assuming the total O was 1 unit, the Ti amount can be calculated as 0.361 unit. Based on this and the O

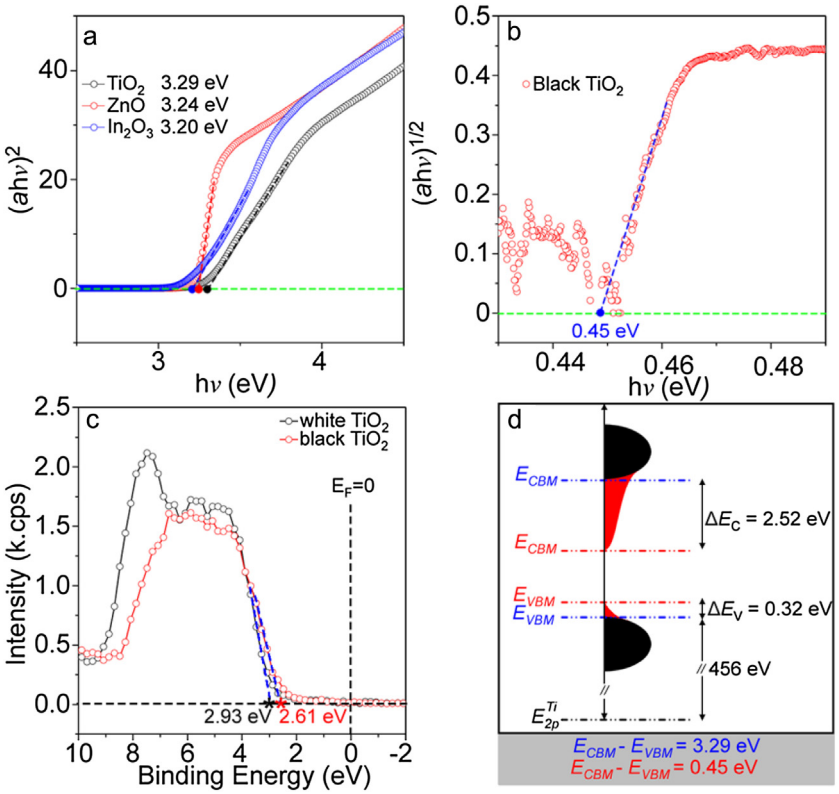

Fig. 9. Characterizations of MO NCs. (a) Tauc plots of as-received TiO_2, ZnO and In_2O_3 NCs, derived from their UV/Vis absorption spectra (Fig. S6a). The optical band gap of NCs was estimated based on the equation $(\alpha h\nu)^n = c(h\nu - E_g)$, where c is a constant, α is the absorption coefficient (here the absorbance was used directly), E_g is the band gap, and n equals 2 and ½ respectively for a direct and indirect transition. E_g is obtained by extrapolating the linear region of plots of $(\alpha h\nu)^2$ *versus* energy ($h\nu$) [30,33]. (b) Tauc plot of black TiO_2 NCs near the absorption tail region. $n = 1/2$ since the defect related gap is an indirect transition. (c) Valence band XPS spectra of TiO_2 NCs. E_F is the fermi energy. (d) A diagram showing the band structure change of TiO_2 due to surface disorder. E_{CBM} and E_{VBM} are respectively the energy level of conduction band minimum and valence band maximum.

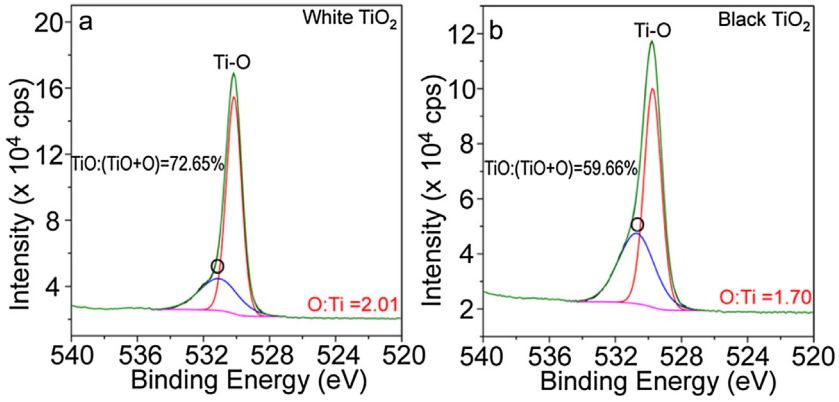

Fig. 10. O1s XPS of (a) white TiO_2 and (b) black TiO_2.

from Ti-O [72.65% (0.7265 unit) of the total O], the ratio of O (from Ti-O):Ti in white TiO_2 NCs was determined as 2.01. By using the same method, the ratios of Ti:O, Zn:O, and In:O in as-prepared NCs were determined as 1.70, 0.88, 1.24, respectively, which were much lower than those in the cases of as-received white NCs (2.01 1.01, 1.52, respectively), suggesting that O vacancies were formed in all the black NCs during their preparation processes (Fig. 10b, Fig. S7). In addition, metallic phases were likely formed in the black NCs. Chen and Liu *et al.* [12,19] calculated the density of states (DOS) of disordered TiO_2 NCs containing O vacancies (similar to our black NCs), and suggested that the disordered surface has some metallic feature. Our XPS results (Fig. S8) showed that the Ti2p, Zn2p and In3d XPS in the cases of black NCs were all shifted (from in the cases of as-received NCs) to lower binding energies due to the O vacancies and surface disorder. Furthermore, the shifted Ti2p, Zn2p and In3d XPS all covered the binding energies of their metallic phases (Fig. S8), suggesting that metallic phases were likely formed in as-prepared black NCs. Electrochemical impedance spectroscopy (EIS) was also used to further characterize as-received and as-prepared black NCs (Fig. S9a). The results confirmed the evident decrease in charger transfer resistance (Rct) in the case of engineered surface disorder, corresponding well with the above results. The formation of new metallic phases improved the electrical conductivity of NCs, making the black NCs highly suitable for a photocatalytic process, in which case, the photon generated electrons at CB could be readily delivered to the surface of NCs for catalysis. TiO_2, ZnO

and In_2O_3 have absolute CB potentials at −0.34, −0.35 and −0.64 V (NHE) respectively [38,39], all of which are more negative than the standard redox potential E ($O_2/O_2^{\bullet-}$ = −0.33 V *versus* NHE, pH = 7) [39,40]. The quantum confinement effects (the optical band gap was slightly larger than that reported [39,40]) for these small NCs) likely lifted up the CB, making it more negative, and making the black NCs more capable of generating active $^{\bullet}O_2^-$ radical, and facilitating the formation of $^{\bullet}$OH. The VBs of these NCs are also more positive than the redox potential of $OH^-/^{\bullet}OH$ (+1.89 V), meaning that the black NCs also could generate $^{\bullet}$OH radicals during the photocatalysis process, which was highly effective in degrading MB (redox potential ~100 mV) and methylene orange (redox potential ~67 mV) under solar light irradiation. In as-prepared black NCs, continuous defect levels below the CB were also generated, which might be lower than the standard redox potential E^0. Liu *et al.* confirmed that these defect levels were highly localized and could improve the separation of electron-hole pairs during photo-chemical processes [41]. This was found by our photo-current tests (Fig. S9b, the photo-generated currents in all the cases of black NCs were considerably improved (over 15–20 times) from those in the cases of as-received NCs, under solar light irradiation). The new defect levels increased photo-conversion of the NCs, as was suggested by the IPCE measurement (Fig. S9c). Besides the increased IPCE at wavelength of 350–400 nm (Fig. S9c), black NCs were active in the wavelength >400 nm (with IPCE ~2%), which was different from the original NCs (IPCE ~0%). It was suggested that the electrons in the formed defect levels could be excited to the CB of NCs, making the formation of $^{\bullet}O_2^-$ and $^{\bullet}$OH more easily with long wavelength irradiation [42]. In addition, the surface areas of black NCs were slightly larger than those of as-received NCs, which could also favour the photocatalytic reaction (Fig. S9d). The combination of all the features described above made black NCs highly active in the degradation of MB and methylene orange under solar light irradiation.

4. Conclusions

In this work, we have developed a simple but universal method to make semiconductive metal oxide (MO) nanocrystals (NCs) that are photoactive in nearly the full range of solar spectrum. This method relies on the reaction (1–2 h) between MO (TiO_2, ZnO and In_2O_3) NCs and potassium (K) under vacuum conditions at a heating temperature between 140 and 170 °C. Due to the high reactivity of solid and molten K, O-containing surface of MO could be readily reacted, resulting in black MO-NCs with disordered surface and significant oxygen (O) vacancies. Meanwhile, the semiconductive cores of these MO-NCs remained and new metallic phases were likely formed, which narrowed effectively the band gaps, enabled as-prepared black NCs to adsorb full solar irradiation and benefited the separation of electron-hole pairs during a photocatalytic process. As an example, we examined the photocatalytic activities of as-prepared black MO-NCs in photo-degradations of MB and methylene orange under solar light irradiation. The results indicated that they performed far better than their un-modified (as-received) counterparts. The principle demonstrated here could be readily extended to the broader family of MOs beyond the NCs (TiO_2, ZnO and In_2O_3) investigated here. Consequently, a range of highly efficient materials could be developed for important photo-chemical (*e.g.* photocatalysis) and photo-physical applications (*e.g.* solar-cell).

Acknowledgement

We thank the National EPSRC XPS Users' Service (NEXUS) at the Newcastle University (UK) for the assistance with XPS characterizations.

Appendix A. Supplementary data

Supplementary data associated with this article can be found, in the online version, at http://dx.doi.org/10.1016/j.apcatb.2016.10.054.

Notes and references

[1] J. Schneider, M. Matsuoka, M. Takeuchi, J. Zhang, Y. Horiuchi, M. Anpo, D.W. Bahnemann, Chem. Rev. 114 (2014) 9919–9986.
[2] M. Wang, J. Ioccozia, L. Sun, C. Lin, Z. Lin, Energy Environ. Sci. 7 (2014) 2182–2202.
[3] X. Bai, L. Wang, R. Zong, Y. Lv, Y. Sun, Y. Zhu, Langmuir 29 (2013) 3097–3105.
[4] J. Gao, X. Lu, J. Wu, S. Xie, T. Zhai, M. Yu, Z. Zhang, Y. Mao, S.C. Wang, Y. Shen, Y. Tong, Sci. Rep. 3 (2013) 1021.
[5] X. Li, Z. Hu, J. Liu, D. Li, X. Zhang, J. Chen, J. Fang, Appl. Catal. B Environ. 195 (2016) 29–38.
[6] M. Zimbone, G. Cacciato, R. Sanz, R. Carles, A. Gulino, V. Privitera, M.G. Grimaldi, Catal. Commun. 84 (2016) 11–15.
[7] X. Bai, L. Wang, R. Zong, Y. Lv, Y. Sun, Y. Zhu, Langmuir 29 (2013) 3079–3105.
[8] X. Zhang, J. Qin, Y. Xue, P. Yu, B. Zhang, L. Wang, R. Liu, Sci. Rep. 4 (2014) 4596.
[9] L. He, T.E. Wood, B. Wu, Y. Dong, L.B. Hoch, L.M. Reyes, D. Wang, C. Kübel, C. Qian, J. Jia, K. Liao, P.G. O'Brien, A. Sandhel, J.Y. Loh, P. Szymanski, N.P. Kherani, T.C. Sum, C.A. Mims, G.A. Ozin, ACS Nano 10 (2016) 5578–5586.
[10] C.M. Lee, C.W. Lai, K.S. Ngai, J.C. Juan, Water Res. 88 (2016) 428–448.
[11] Z. Li, P. Zhang, T. Shao, J. Wang, L. Jin, X. Li, J. Hazard. Mater. 260 (2013) 40–46.
[12] X. Chen, L. Liu, P.Y. Yu, S.S. Mao, Science 331 (2011) 746.
[13] H. Wang, L. Zhang, Z. Chen, J. Hu, S. Li, Z. Wang, J. Liu, X. Wang, Chem. Soc. Rev. 43 (2014) 5234–5244.
[14] X. Chen, L. Liu, F. Huang, Chem. Soc. Rev. 44 (2015) 1861–1885.
[15] J. Lin, J. Shen, R. Wang, J. Cui, W. Zhou, P. Hu, H. Liu, J. Wang, R.I. Boughton, Y. Yue, J. Mater. Chem. A 21 (2011) 5106.
[16] C. Chen, C. Liao, K. Hsu, Y. Wu, J.C.S. Wu, Catal. Commun. 12 (2011) 1307–1310.
[17] G. Wu, T. Nishikawa, B. Ohtani, A. Chen, Chem. Mater. 19 (2007) 4530–4537.
[18] F. Dong, S. Guo, H. Wang, X. Li, Z. Wu, J. Phys. Chem. C 115 (2011) 13285–13292.
[19] X. Chen, L. Liu, Z. Liu, M.A. Marcus, W.-C. Wang, N.A. Oyler, M.E. Grass, B. Mao, P.-A. Glans, P.Y. Yu, J. Gao, S.S. Mao, Sci. Rep. 3 (2013) 1510.
[20] H. Wang, T. Lin, G. Zhu, H. Yin, X. Lü, Y. Li, F. Huang, Catal. Commun. 60 (2015) 55–59.
[21] G. Zhu, H. Yin, C. Yang, H. Cui, Z. Wang, J. Xu, T. Lin, F. Huang, ChemCatChem 7 (2015) 2614–2619.
[22] W. Zhou, W. Li, J. Wang, Y. Qu, Y. Yang, Y. Xie, K. Zhang, L. Wang, H. Fu, D. Zhao, J. Am. Chem. Soc. 136 (2014) 9280–9283.
[23] A. Naldoni, M. Allieta, S. Santangelo, M. Marelli, F. Fabbri, S. Cappelli, C.L. Bianchi, R. Psaro, V. Dal Santo, J. Am. Chem. Soc. 134 (2012) 7600–7603.
[24] W. Hu, W. Zhou, K. Zhang, X. Zhang, L. Wang, B. Jiang, G. Tian, D. Zhao, H. Fu, J. Mater. Chem. A 4 (2016) 7495–7502.
[25] X. Liu, Z. Xing, H. Zhang, W. Wang, Y. Zhang, Z. Li, X. Wu, X. Yu, W. Zhou, ChmSusChem 9 (2016) 1118–1124.
[26] F. Teng, M. Li, C. Gao, G. Zhang, P. Zhang, Y. Wang, L. Chen, E. Xie, Appl. Catal. B Environ. 148–149 (2014) 339–343.
[27] G. Panomsuwan, A. Watthanaphanit, T. Ishizaki, N. Saito, Phys. Chem. Chem. Phys. 17 (2015) 13794–13799.
[28] A. Sinhamahapatra, J.-P. Jeon, J.-S. Yu, Energy Environ. Sci. 8 (2015) 3539–3544.
[29] L. Lin, S. Zhang, Chem. Commun. 48 (2012) 10177–10179.
[30] L. Lin, Y. Xu, S. Zhang, I.M. Ross, A.C.M. Ong, D.A. Allwood, Small 10 (2014) 60–65.
[31] L. Lin, Y. Xu, S. Zhang, I.M. Ross, A.C.M. Ong, D.A. Allwood, ACS Nano 7 (2013) 8214–8223.
[32] L. Lin, N. Miao, Y. Wen, S. Zhang, P. Ghosez, Z. Sun, D.A. Allwood, ACS Nano 10 (2016) 8929–8937.
[33] J.I. Pankove, Optical Processes in Semiconductors, Prentice-Hall, New Jersey, 1971.
[34] A. Ghish, R.N.P. Choudhary, J. Phys. D Appl. Phys. 42 (2009) 075416.
[35] Z. Li, P. Zhang, T. Shao, J. Wang, L. Jin, X. Li, J. Hazard. Mater. 260 (2013) 40–46.
[36] S.A. Ansari, M.M. Khan, S. Kalathil, A. Nisar, J. Lee, M.H. Cho, Nanoscale 5 (2013) 9238–9246.
[37] D.O. Scanlon, C.W. Dunnill, J. Buckeridge, S.A. Shevlin, A.J. Logsdail, S.M. Woodley, C.R.A. Catlow, M.J. Powell, R.G. Palgrave, I.P. Parkin, G.W. Watson, T.W. Keal, P. Sherwood, A. Walsh, A.A. Sokol, Nat. Mater. 12 (2013) 798–801.
[38] Y. Xu, M.A.A. Schoonen, Am. Mineral. 85 (2000) 543–556.
[39] N. Boonprakob, N. Wetchakun, S. Phanichphant, D. Waxler, P. Sherrell, A. Nattestad, J. Chen, B. Inceesungvorn, J. Colloid Interface Sci. 417 (2014) 402–409.
[40] X. Fu, W. Tang, L. Ji, S. Chen, Chem. Eng. J. 180 (2012) 170–177.
[41] L. Liu, P.Y. Yu, X. Chen, S.S. Mao, D.Z. Shen, Phys. Rev. Lett. 111 (2013) 065505.
[42] F.B. Li, X.Z. Li, Chemosphere 48 (2002) 1103–1111.